Predictive Membrane Transport Model for Nanofiltration Processes in Water Treatment

Shih-Chieh Tu, Varadarajan Ravindran, Walter Den, and Massoud Pirbazari
Dept. of Civil and Environmental Engineering, University of Southern California, Los Angeles, CA 90089

A membrane transport model was developed for prediction and simulation of membrane filtration (nanofiltration) dynamics with reference to permeate flux. It incorporates important phenomenological aspects of membrane transport, such as concentration polarization and gel layer formation, and illustrates the concentration of solutes as foulants in the mass-transfer boundary layer on the membrane surface. Membrane filtration tests using tannic acid as a model organic compound were designed for investigating permeate fluxes, as well as solute concentration profiles for permeates and concentrates. Membrane performance experiments were conducted under various operation conditions by varying several parameters including solute concentrations, transmembrane pressures, and reject flow rates. The tests showed that the NF-45 membrane composed of polypiperazine amide was more susceptible to organic fouling by tannic acid than the NF-70 membrane made of cross-linked aromatic polyamide. These observations were supported by surface-potential measurements that demonstrated higher negative surface charges and greater hydrophilicity for the NF-70 membrane in the presence of tannic acid. The predictive capability of the membrane transport model was evaluated using the results from membrane filtration tests. Model sensitivity studies were conducted to obtain information on effects of various input parameters pertaining to operating conditions and fluid-dynamic regimes.

Introduction

Membrane applications in water and wastewater treatment have grown rapidly since the development of synthetic asymmetric membranes by Loeb and Sourirajan in 1960. Recent global emphasis on membrane processes can be attributed to the following factors: (1) increased regulatory pressure to provide better treatment for potable waters and wastewaters; and (2) increased demand for water requiring exploitation of water resources of lower quality than those relied upon previously (Mallevialle et al., 1996). Membrane processes cover a wide spectrum of water and wastewater treatment applications, including the following: removal of colloidal particles, microorganisms, natural organic matter (NOM), heavy metals, and nonmetallic inorganics ions from contaminated waters and industrial effluents (Taylor et al., 1987; Ho and Sirkar, 1992; Aim et al., 1993; Koros, 1995). Nanofiltration is mainly employed for the removal of organic and inorganic compounds of molecular weights above 300 Da (Fu et al., 1994; Mallevialle et al., 1996; Braghetta et al., 1997). The primary objective in removing NOM from natural waters is to reduce the potential for disinfection byproduct formation during chlorination.

The economics of membrane filtration processes are largely dependent on the permeate flux (Chellam and Wiesner, 1992, 1997). A serious limitation in such processes is the progressive permeate flux deterioration due to membrane fouling and concentration polarization, two phenomena that affect their overall performance and economics (van den Berg and Smolders, 1988; Pirbazari et al., 1992; Mallevialle et al., 1996). Membrane fouling attributed to sorption of natural organic matter, inorganic compounds, or colloidal matter is important from a water treatment standpoint. The fouling mechanisms causing flux deterioration in various membrane technologies, such as microfiltration, ultrafiltration, nanofiltration, and reverse osmosis, are of different types and charac-

Correspondence concerning this article should be addressed to M. Pirbazari.

ter (Aim et al., 1993; Koros, 1995; Pirbazari et al., 1996). Such mechanisms include concentration polarization on the membrane surface, surface fouling due to adsorption and gel-layer formation, and internal pore fouling due to pore adsorption and pore blocking (Wijmans et al., 1984; van den Berg and Smolders, 1988; Ko and Pellegrino, 1992). In nanofiltration and reverse osmosis applications permeate flux deterioration is mainly attributed to concentration polarization and surface fouling; whereas, in ultrafiltration and microfiltration processes, it can be attributed to internal pore fouling as well. Membrane fouling can be reversible when flux recovery can be achieved by chemical cleaning or fluid dynamics, or irreversible when flux recovery is not possible. This reversible fouling is referred to as ''colmatage'' to be distinguished from irreversible fouling (Chellam and Wiesner, 1992). Recent developments in membrane technologies have led to new *genre* of membranes that operate at lower pressures, offer resistance to fouling, and simultaneously maintain higher solute rejections without sacrificing permeate fluxes (Aim et al., 1993).

Membrane transport of organic compounds and the associated permeate flux decline has been conceptualized by several phenomenological models, including the following: concentration polarization model, osmotic pressure model, and resistance-in-series model (Wijmans and Baker, 1995; Ko and Pellegrino, 1992; Nabetani et al., 1990; Nakao et al., 1986; van Boxtel et al., 1991; and van den Berg and Smolders, 1988). These models have been conceptualized for predicting or simulating permeate flux decline under steady-state conditions. The model discussed in this article is developed for predicting or simulating permeate flux decline under unsteady-state and/or transient-state conditions. More specifically, this study investigates permeate flux decline due to the combined effects of gel-layer and concentration-polarization-layer formations, primarily attributed to organic foulants. Although the developed model is applied to nanofiltration in this article, this approach can be extrapolated to other membrane processes as well.

In recent years, development of predictive/simulative models in water and wastewater treatment has become an important research area. The utility of such models is greatly reinforced by the following aspects: predicting/simulating the process performance and dynamics, accomplishing efficient and economical process design, and achieving process upscaling from laboratory-scale to pilot-scale, and eventually to full-scale operation. More specifically, these models contribute to efficient and economic planning and design of treatment systems for specific applications. With reference to membrane processes, performance prediction/simulation of permeate fluxes under various operating conditions is primordial for efficient and cost-effective process design (Bhattacharyya, et al., 1990). These models facilitate the forecasting of process dynamics under different operating conditions, and indeed conserve a great deal of time, effort, and finance involved in planning and design. Traditionally, such planning and design involves extensive and expensive pilot-scale investigations before a process can be developed from laboratory-scale to full-scale. In the present modeling approach, synthesis of laboratory data provides the necessary feedback for verification of the predictive capability of such models, and implementation of model refinements whenever necessary. This technique reduces the scope of elaborate, expensive, and time-consuming pilot-scale studies, which would otherwise be required prior to full-scale design. It also provides the means to obtain performance predictions/simulations under a variety of process operating conditions, and facilitates process upscaling through dimensional analysis and similitude techniques. The objective in employing specific modeling approaches and protocols is to economize the time and effort involved in process design for specific applications by reducing considerably the volume of pilot-scale studies. Such modeling approaches prove useful in evaluating the effects of various operational variables and process parameters on the overall process dynamics, and smoothen the transition from laboratory-scale conception to pilot-scale demonstration, and subsequently to full-scale implementation.

The primary objective of this research is to conceptualize and develop a membrane transport model incorporating the concentration polarization and gel-layer formations for performance prediction of membrane processes for removal of natural organics. A plate-and-frame membrane system is employed to perform the filtration tests to remove tannic acid, a model compound representing natural organic matter, under different operating conditions including transmembrane pressure, reject flow rate, and model compound concentration. The predictive capability of the model is evaluated based on comparisons with experimental results under a variety of operating conditions. Model sensitivity analysis is performed to obtain information on the influence of input parameters such as gel-layer and concentration polarization characteristics on the membrane transport model simulations.

Development of Predictive Mathematical Modeling

Fundamental aspects and concentration profiles of the proposed model

A serious limitation in the operation of membrane processes is the progressive deterioration in permeate flux due to several phenomena in, on, and near the membrane, a factor that affects the overall process economics. According to Darcy's law, permeate flux (J_v) decline is caused by decreased driving forces and/or increased resistances (van den Berg and Smolders, 1988; Ho and Sirkar, 1992). The driving forces for the membrane processes include the following: applied pressure (ΔP), concentration gradient (ΔC), and/or temperature difference (ΔT). Membrane permeate flux can be described by the relation

$$\text{Flux } J_v = \frac{\text{Driving force(such as } \Delta P, \Delta C, \text{ or } \Delta T)}{\text{Viscosity} \times \text{total resistance}}. \quad (1)$$

Permeate flux decline can be categorically attributed to two major phenomena, namely, concentration polarization (reversible and directly occurring phenomena) and fouling (irreversible and long-term phenomena) (van den Berg and Smolders, 1988; Ko and Pellegrino, 1992). The resistances occurring in membrane processes could be caused by the membrane, concentration polarization, internal pore fouling, and gel-layer formation.

The resistance of the virgin membrane (R_m) is a constant factor during filtration. Concentration polarization resistance

arises due to solute retention by the membrane when solvent transport is facilitated. Solute accumulates on the membrane surface and forms a layer at the membrane interface with a relatively high concentration. The resistance due to the concentration polarization layer (R_{cp}) increases during membrane filter operation until the system reaches steady state. Concentration polarization also results in higher osmotic pressure ($\Delta\pi$) associated with the membrane, causing a decrease in the driving force (Wijmans et al., 1984; Nabetani et al., 1990; van Boxtel et al., 1991; Ko and Pellegrino, 1992). For some cases, the solution concentration at the membrane interface can reach certain high values, and will progressively evolve into a gel layer accumulating on the membrane surface (R_g) (Wijmans et al., 1984; van den Berg and Smolders, 1988; van Boxtel et al., 1991). Internal pore fouling occurring inside the membrane can also lead to permeate flux decline (R_{in}).

In cases where foulant molecules are larger than membrane pores, internal pore fouling will not occur, but surface fouling will be experienced. The foulant molecules will not penetrate the membrane, but would either be retained on the membrane surface and/or concentrated in the reject flow. From this perspective, the model compound used in this study has a molecular weight of 1700 while the nanofiltration membrane pore size is 300 Daltons. Accordingly, the proposed model neglects resistance due to internal pore fouling, and essentially focuses on resistance due to the clean membrane, concentration polarization, and gel formation. Concentration profiles of the proposed model during the membrane filtration processes involve two stages: (a) before gel-layer formation, and (b) after gel-layer formation (Figure 1). Here, C_b is the bulk solution concentration, C_p is the permeate concentration, C'_m is the solute concentration at the membrane surface inside the membrane, and δ is the thickness of the concentration polarization layer. The concentrations of for permeate and the solution within the membrane region are assumed to be zero for theoretical considerations. At the beginning of membrane filtration processes, the solute concentration at membrane surface (C_m) is insignificant, and hence no gel layer is formed (Figure 1a). The permeate flux decline is mainly caused by the concentration polarization layer resistance. After a short period of time, the solute concentration at the membrane surface reaches the limiting gel-layer concentration (C_g), and gel-layer formation commences (Figure 1b). The thickness of gel layer increases until the system reaches steady state, at which stage, the permeate flux decline is mainly caused by the gel-layer resistance.

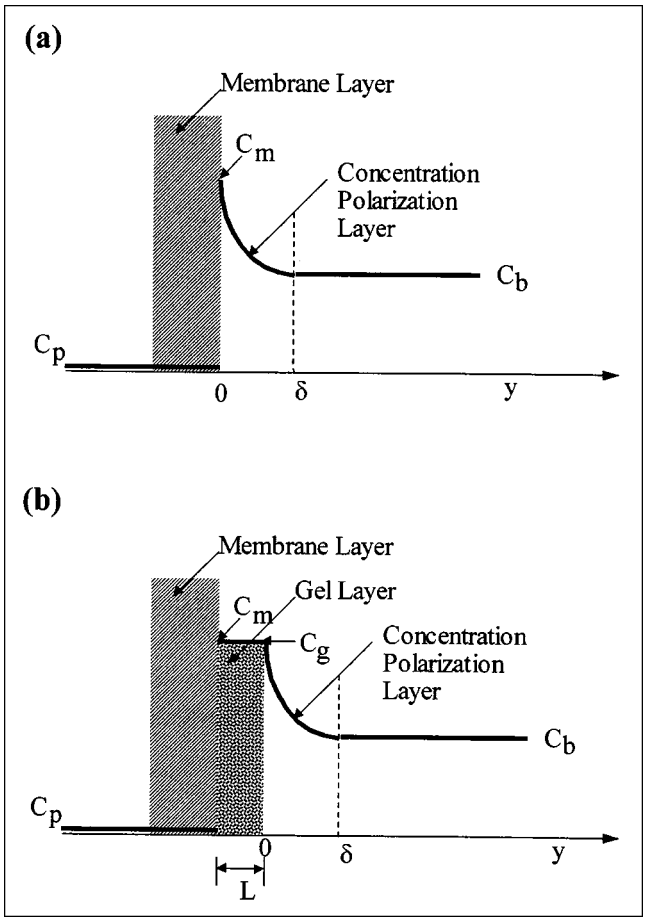

Figure 1. Concentration profiles of the proposed model without internal fouling.

(a) Before the gel-layer formation ($C_m < C_g$); (b) after the gel-layer formation ($C_m = C_g$).

Model framework

The fundamental membrane transport model equation is the classic advection–diffusion equation discussed in detail by Bird et al. (1960). The general form of the advection–diffusion equation for a binary system (solute/solvent system) can be written as shown below:

$$\frac{\partial C}{\partial t} + \nu \cdot \nabla C = D\nabla^2 C, \tag{2}$$

where C is the concentration of the solute and D is the diffusivity of the solute in the solvent phase (water).

The proposed membrane transport model only considers the solute mass transfer in the region between the membrane surface and membrane cell wall, and disregards internal pore fouling (van den Berg and Smolders, 1988; Wiesner and Chellam, 1992; Von Meien and Nobrega, 1994). The mathematical representation of solute transport through the membrane system in the region between the membrane and the cell wall is illustrated in Figure 2, wherein the control volume for advection and back diffusion is shown (marked A). According to the rectangular Cartesian coordinate system, the bulk solution flows between the membrane and membrane cell wall in the x-direction. The solute transport occurs in the y-direction, controlled by advection from bulk solution to the membrane, and diffusion from membrane surface back to the bulk solution. It must be noted that the advective and diffusive transport mechanisms are not exactly balanced before the system reaches steady state, and consequently the concentration polarization and gel layers exhibit variable thickness with time. The advection–diffusion equation (Eq. 2) developed for the control volume shown in Figure 2 can be simplified using the following assumptions:

1. No concentration gradient exists in the z-direction; that is, $\partial C/\partial z$ and $\partial^2 C/\partial z^2$ are equal to zero.

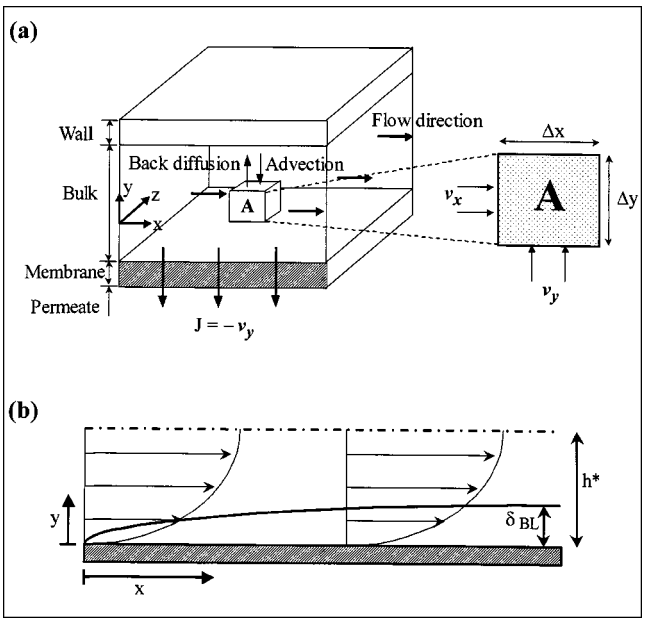

Figure 2. Mathematical representation of mass transport in the membrane module.

(a) Solute transport through the membrane system in the region between the membrane and the cell wall, showing the control volume for advection and back diffusion; (b) hydrodynamic boundary layer in the flow channel.

2. The concentration gradient in the direction of product flow ($\partial C/\partial x$) can be considered negligible in comparison with $\partial C/\partial y$.

Using the preceding assumptions and considering the relation $v_y = -J_V$, Eq. 2 can be transformed as

$$\frac{\partial C}{\partial t} - J_v \frac{\partial C}{\partial y} = D \frac{\partial^2 C}{\partial y^2}. \tag{3}$$

As illustrated in Figure 1, the boundary conditions for the preceding equation (Eq. 3) can be written as follows. For the temporal and spatial stages before the gel-layer formation ($C_m < C_g$), Figure 1a,

$$\text{at} \quad t = 0, \quad C = C_{m,0} = C_{b,0}$$
$$\text{at} \quad y = \delta, \quad C = C_b$$
$$\text{at} \quad y = 0, \quad J_v C_m = -D\left(\frac{\partial C}{\partial y}\right)_{y=0}.$$

For the temporal and spatial stages after the gel-layer formation ($C_m = C_g$), Figure 1b,

$$\text{at} \quad y = L + \delta, \quad C = C_b$$
$$\text{at} \quad y \le L, \quad C = C_g.$$

Under steady-state conditions ($dC/dt = 0$), the solution to Eq. 3 with the boundary conditions becomes

$$J_v = \frac{D}{\delta} \ln \frac{C_m}{C_b} = k \ln \frac{C_m}{C_b}, \tag{4}$$

where k represents the mass-transfer coefficient for solute transport through the membrane cell. After the gel-layer formation, the solute concentration on the membrane surface will equal the gel-layer concentration ($C_m = C_g$), and Eq. 4 can therefore be written as

$$J_v = k \ln \frac{C_m}{C_b} = k \ln \frac{C_g}{C_b}. \tag{5}$$

Membrane fouling can be classified into two components, namely, external fouling and internal fouling. External fouling occurs on the top surface of the membrane due to the accumulation of pollutants that do not enter the pores, whereas internal fouling occurs within the internal pore structure due to pore deposition and sorption of pollutant molecules. The membrane permeate flux (J_v) can be described by the fundamental relation

$$J_v = \frac{\text{Driving force}}{\text{Viscosity} \times \text{total resistance}} = \frac{\Delta P - \Delta \pi}{\mu\left(R_m + R_g + R_{cp} + R_{in}\right)}, \tag{6}$$

where ΔP is the applied pressure, $\Delta \pi$ is total osmotic pressure between the bulk solution and permeate solution, $\Delta P - \Delta \pi$ represents the total driving force, $(R_m + R_g + R_{cp} + R_{in})$ denotes the total resistance of the system, and μ is the feed solution dynamic viscosity. Neglecting the effects of internal pore fouling resistance (R_{in}), Eq. 6 can be written as

$$J_v = \frac{\Delta P - \Delta \pi}{\mu\left(R_m + R_g + R_{cp}\right)}. \tag{7}$$

Differentiating Eq. 7 with respect to time, and regarding ΔP, μ, and R_m as constants, we have

$$(\Delta P - \Delta \pi) \times \frac{dJ_v}{dt} + \mu J_v^2 \times \left(\frac{dR_g}{dt} + \frac{dR_{cp}}{dt}\right) + J_v \frac{d\Delta \pi}{dt} = 0, \tag{8}$$

where the osmotic pressure variation with time is given by the following equations based on virial coefficients (Haynes et al., 1992; Nabetani et al., 1990)

$$\Delta \pi = \frac{RT}{M}\left(C_b + B_2 C_b^2 + B_3 C_b^3 + \cdots\right) \tag{9}$$

and

$$\frac{d\Delta \pi}{dt} = \frac{RT}{M}\left(1 + 2B_2 C_b + 3B_3 C_b^2 + \cdots\right)\frac{dC_b}{dt}. \tag{10}$$

The concentration polarization resistance R_{cp} referred to in Eqs. 7 and 8 can be estimated by a modification of the power law suggested by several investigators (van Boxtel et

al., 1991; Pradanos et al., 1992; Akay and Wakeman, 1993; Timmer et al., 1994) as shown below

$$R_{cp} = av^b \Delta P^c C_b^d C_f^e. \tag{11}$$

In the preceding equation, the concentration polarization resistance R_{cp} is considered as a time-dependent variable until the system reaches steady state. Hence, differentiating the preceding relation with respect to time results in

$$\frac{dR_{cp}}{dt} = adv^b \Delta P^c C_b^{d-1} C_f^e \frac{dC_b}{dt}. \tag{12}$$

The gel-layer resistance R_g also manifests temporal variation until steady state is reached. The progressive accumulation of solute on the membrane (gel-layer formation) is due to the difference between the net solute transport from the bulk solution to the membrane and solute back-diffusion from the membrane to the bulk solution (van Boxtel et al., 1991; Timmer et al., 1994), and is represented as follows

$$\rho_g \frac{dL_g}{dt} = J_v C_b - C_b k \ln \frac{C_g}{C_b}, \tag{13}$$

where L_g and ρ_g represent thickness and density of the gel layer, respectively. Considering a linear relation between the gel-layer resistance and the thickness of the gel layer

$$R_g = \epsilon L_g, \tag{14}$$

where ϵ is the resistance per unit of the gel-layer thickness. From Eqs. 13 and 14, the resistance of gel-layer variation with time can be written as

$$\frac{dR_g}{dt} = \frac{\epsilon}{\rho_g} C_b J_v - \frac{\epsilon k}{\rho_g} C_b \ln \frac{C_g}{C_b}. \tag{15}$$

The boundary conditions for the preceding differential equations (Eqs. 8, 12, and 15) are the following:

For the Stage Before Gel-Layer Formation ($C_m < C_g$). At any time before gel-layer formation

$$L_g = R_g = \frac{dR_g}{dt} = 0$$

$$\text{at } t = 0,\ J_v = J_{v,0}, \text{ and } R_{cp,0} = av^b \Delta P^c C_{b,0}^d C_f^e.$$

For the Stage After Gel-Layer Formation ($C_m = C_g$)

$$\text{at } t = 0,\ L_g = R_g = 0$$

Aqueous diffusion coefficients of the natural organic matter in dilute solution can be estimated by the Stokes-Einstein equation (Cornel et al., 1986)

$$D = \frac{\bar{k}T}{6\pi\mu r} = \frac{\bar{k}T}{6\pi\mu}\left(\frac{3}{4\pi}\frac{MW}{\rho_A N}\right)^{-1/3} = \frac{\bar{k}T}{3\mu}\left(6\pi^2 \frac{MW}{\rho_A N}\right)^{-1/3}, \tag{16}$$

where $\bar{k}$ is the Boltzmann constant, T is the absolute temperature, μ is the dynamic viscosity, r is the molecular radius, N is the Avogadro's number, and ρ_A is the density of the molecule. The Stokes-Einstein correlation is well established for estimating free liquid (aqueous phase) diffusivities of polymers with molecular weights over 1,000 Daltons, and globular proteins composed of cross-linked molecules (Polson, 1950; Young et al., 1980). It has been successfully employed by Cornel et al. (1986) for estimating the free liquid diffusivity of humic acid, and can generally be used for macromolecular mixtures, including complex organic molecules and unhydrated polymers such as humic and tannic acids. This equation has its roots in the kinetic theory of molecules, and so the estimated molecular diffusivities represent ensemble averages of various thermodynamic properties corresponding to different molecular-weight fractions in organic mixtures. The diffusion coefficient evaluated for tannic acid was 2.635×10^{-10} m^2/s.

The mass-transfer coefficient k can be calculated from Sherwood correlations of the form used by several researchers (Bird et al., 1960; van den Berg et al., 1989; Pradanos et al., 1992, 1995; von Meien and Nobrega, 1994):

$$Sh = kd_h/D = pRe^q Sc^r, \tag{17}$$

where d_h is the hydraulic diameter of the system, D is the diffusion coefficient, Re is the Reynolds number ($Re = \rho v d_h/\mu$), Sc is the Schmidt number ($Sc = \mu/\rho D$), and p, q, and r are constants depending on the hydraulic regimes. Wiley et al. (1985) and van den Berg et al. (1989) used the following correlations for membrane filtration systems operating under laminar flow conditions ($Re \leq 2{,}000$).

$$L < L^*: Sh = 0.664\ Re^{0.5} Sc^{0.33} (d_h/L)^{0.33} \tag{18}$$

$$L > L^*: Sh = 1.86\ Re^{0.33} Sc^{0.33} (d_h/L)^{0.33}, \tag{19}$$

where the entry length L^* is given by the relation $L^* = 0.029 d_h Re$. These correlations establish the dependence of the mass-transfer coefficient on fluid dynamics of the system and the solute/solvent characteristics for positions represented by L less than or greater than the characteristic entry length L^* required for fully developed flow. While the Reynolds number characterizes the fluid flow and momentum transport along the membrane surface in relation to inertial forces, the Schmidt number describes the diffusion transport of solute (foulant) molecules to and from the membrane surface under these conditions.

The membrane transport model further emphasizes the role of solute concentrations in the gel layer and the hydro-

dynamic boundary layer in relation to that in the bulk fluid, an important aspect for evaluating the fouling potential. The solute concentration within the boundary layer is estimated by the modeling approach of Trettin and Doshi (1980). The purpose of this modeling effort is to evaluate the impact of hydrodynamic boundary layer on gel-layer formation, an aspect not studied in depth because of experimental difficulties associated with measuring boundary-layer properties during the transient-state operation. The theoretical computations presented below are applicable for estimating boundary-layer thickness for tubular membrane modules, and are based on results from classic heat- and mass-transfer problems adopted by Doshi and coworkers (Doshi, 1980; Trettin and Doshi, 1980). Analogous to this method, the hydrodynamic boundary-layer characteristics for laminar flows with parallel-plate geometry can also be established. By rearranging Eq. 4 and by assuming that the flow is fully developed over the entire length of the membrane plate, the velocity and concentration profiles of the feed flow can be written as shown below

Velocity profile: $$u = 4u_0\left[\left(\frac{y}{h}\right) - \left(\frac{y}{h}\right)^2\right] \tag{20}$$

Concentration profile: $$C = C_0 \exp\left[\frac{V_w}{D}(\delta_{BL} - y)\right] \tag{21}$$

In the preceding relations, h is the channel height between the plates, y is the coordinate in the vertical direction, u_0 represents axial flow velocity at the center of the plate ($y = h/2$), and δ_{BL} represents the boundary layer thickness, C_0 is the solute concentration at the center of the plate ($y = h/2$). This boundary-layer thickness can be estimated by adapting the Leveque heat-transfer solution under appropriate flow conditions and geometry

$$V_w = 1.18\left(\frac{2D^2u}{hL}\right)^{1/3} \ln\frac{C_g}{C_m}. \tag{22}$$

Matching Eq. 5 with Eq. 22 and substituting for $k = D/\delta$, one would obtain a dimensionless boundary-layer thickness as follows

$$\frac{\delta_{BL}}{h} = 0.424\left(\frac{4DL}{uh^2}\right)^{1/3}. \tag{23}$$

Two important properties of the hydrodynamic boundary layer are the flow fraction (f) and concentration within the boundary layer (C_{BL}), which can be mathematically defined and calculated by the following integrals

Volumetric flow fraction: $$f = \frac{\int_{y=0}^{y=\delta} yu\,dy}{\int_{y=0}^{y=h/2} yu\,dy} \tag{24}$$

Boundary-layer concentration: $$C_{BL} = \frac{\int_{y=0}^{y=\delta} yuc\,dy}{\int_{y=0}^{y=\delta} yu\,dy}. \tag{25}$$

The ratio of the solute concentration within the boundary layer to that in the bulk fluid C_{BL}/C_0 can be termed as the concentration factor. In the present study, the concentration factor is evaluated under various fluid dynamic conditions. The approximate solutions for Eq. 24 and Eq. 25, with incorporation of Eq. 20 and Eq. 21 in appropriate places, are presented as follows:

$$f = \frac{1}{5}(8a^3 - 3a^4) \tag{26}$$

$$\frac{C_{BL}}{C_0} = \frac{12(\delta_{BL} - h)}{B\delta_{BL}(4h-3)} - \frac{24(3 - Bh)}{B^4\delta_{BL}^3(4h-3)}e^{B\delta_{BL}}, \tag{27}$$

where $a = 2\delta_{BL}/h$ and $B = V_w/D$. It is important to evaluate the flow fraction and the concentration factor under various fluid dynamic regimes to obtain a good understanding of the boundary-layer effect with reference to the gel-layer and concentration-polarization-layer formation in membrane processes.

Numerical technique for model simulations

The model is composed of a partial differential equation (advection–diffusion) and a set of time-dependent equations (R_g, J_v, R_{cp}, C_b). These equations, along with their corresponding initial and boundary conditions, were solved simultaneously by adopting the explicit finite difference scheme developed in MATLAB language (Lindfield and Penny, 1995). Initially, a network of grid points was deployed throughout the region of interest occupied by the independent variables (y, t). Then, in the context of the explicit finite difference scheme, two methods were employed for the computation: Euler approximations of the first-order time derivatives of time-dependent variables, and the central-difference technique for the first- and second-order spatial derivatives (Weber and Crittenden, 1975; Smith, 1985; Chapra and Canale, 1988; Sewell, 1988; Kim and Pirbazari, 1989; Schiesser, 1991; Ravindran et al., 1996). The discretized equations were then solved iteratively until a convergence criterion was satisfied for the bulk solution concentration and the permeate flux. This computer program has the versatility to model the changes in permeate fluxes, reject solution concentrations, and concentration polarization and gel-layer resistances with respect to time.

Materials and Methods

Membranes and model compounds

The membranes tested in these studies were chosen from commercially available industrial products. The nanofiltration membranes used in the membrane performance tests

Table 1. Characteristics of Membranes Using in this Study

Membrane Type	NF-45	NF-70
Membrane material	Polypiperazine amide	Cross-linked aromatic polyamide
Molecular weight cutoff (MWCO)	~ 200–300 Da	~ 200–300 Da
pH operating range	2–11	3–9
*Contact angle		
Clean membrane	45°	27.3°
Exposed to 30 mg/L tannic acid	50.2°	34.1°
Maximum temp., °C	45	35
Maximum pressure, MPa	4.1	1.7
*Surface charge or surface potential (at pH of 6-9)		
Deionized distilled water	−22 mV to −33 mV	−22 mV to −33 mV
Tannic acid, 10 mg/L	−17 mV to −20 mV	−34 mV to −40 mV
Water flux (at 1.0 MPa, clean membrane)	56 $L/m^2 \cdot h$	92 $L/m^2 \cdot h$

Source: Redondo and Lanari, 1997; Van der Bruggen et al., 1998; Sadr Ghayeni et al., 1998.
*Determined in this study.

were FilmTec NF-45 and NF-70 thin-film composite membranes (FilmTec Corporation, Dow Chemical Co., Midland, MI). These thin-film composite membranes are cast from polyamide material on a polysulfone support. These two types of membranes were chosen because they have different adsorption affinity and surface hydrophobicity for the test compound. Some important characteristics of the NF-45 and NF-70 membranes are summarized in Table 1.

Tannic acid was chosen for these tests to represent natural organic compounds present in surface and ground waters. It is a hydrophilic organic compound that contains both saccharide and aromatic acid components of significance in surface waters (Mallevialle et al., 1989; Crozes et al., 1993; Dentel et al., 1995). Tannic acid ($C_{76}H_{52}O_{46}$, molecular weight = 1701.22) of ACS reagent-grade purity (Sigma Chemical Co., St. Louis, MO) was used as a moderate molecular-weight model compound. It is a derivative of glucose in which five hydroxyl groups are substituted for digalic acids, and thus contains a large number of phenolic hydroxyl groups. Aqueous solutions of tannic acid were prepared in deionized distilled water with approximately phosphate buffer, and three concentrations of 2.5, 5, and 10 mg/L were employed.

Membrane filtration experiments

A plate-and-frame membrane system was employed in the membrane filtration experiments, which is illustrated in Figure 3. The feed solution was pumped from the feed tank to the stainless-steel plate-and-frame membrane cell (SEPA CF membrane cell; Osmonics, Minnetonka, MN), as shown in the figure.

The system was maintained under high transmembrane pressures of 750–1,500 kPa (110–220 psi). The feed solutions consisted of tannic acid at concentrations in the range of 0–10 mg/L. The feed was allowed to flow into the plate-and-frame cell, and the flow rate into the cell was controlled by the recirculation flow rate into the feed tank. Permeate and reject flow rates were continuously measured. The transmembrane pressure was carefully monitored and maintained at the desired levels. The temperature of the feed was maintained at 20°C, and the feed flow velocity was varied from 0.4 cm/s to 1 cm/s. The permeate and the concentrates were collected at their corresponding outlets as shown in the figure. Samples were obtained from the permeates and the concentrates, and were analyzed for tannic acid concentrations to evaluate the solute rejection characteristics of the membrane.

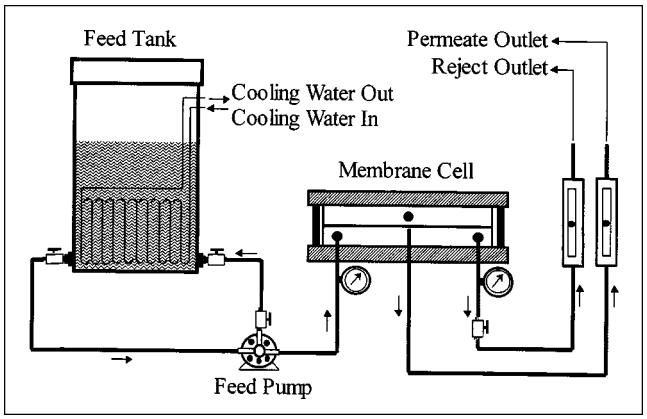

Figure 3. Cross-flow membrane experimental setup.

In order to measure the osmotic pressures of the model compound solutions, a modified version of the membrane osmometer cell was employed (Vilker et al., 1981; Nabetani et al., 1990). Osmotic pressures of solutions with different solute concentrations were measured in this study.

Analytical techniques

The concentrations of tannic acid in aqueous solutions were determined by ultraviolet-visible spectroscopy using a Perkin-Elmer Model Lambda 4 A UV-visible spectrophotometer (Perkin-Elmer Corp., Norfolk, CT) with a characteristic wavelength of 273.2 nm (Crozes et al., 1993; Rivera-Utrilla et al., 1993; Dentel et al., 1995). A range of 0 to 50 mg/L was deemed sufficient to encompass the concentrations of natural organic compounds encountered in natural waters. The total organic carbon (TOC) concentrations of tannic acid were measured using a Shimadzu Model TOC-5000 TOC Analyzer (Shimadzu Scientific Instruments, Columbia, MD), as described in Standard Methods (1995). Contact angle and surface potential (zeta potential) measure-

ments were also conducted for the two membranes. The relevant analytical methods can be found elsewhere (Tu et al., 1997).

Results and Discussions

Model parameters estimation

Parameters estimation for the membrane transport model was an important aspect of this study. As the compositions of the membranes were proprietary, and their material properties were not available, results from membrane filtration tests were employed for parameter estimation. These parameters included the following: various resistances to transport such as the intrinsic membrane resistance, R_m, total permeate resistance, R_{Total}, resistance of the concentration polarization layer, the osmotic pressure, $\Delta\pi$, the transmembrane pressure, ΔP, the variation of the gel layer resistance, R_g, with respect to time, the mass transfer coefficient, k, and the specific gel layer resistance, ϵ. The parameter estimation techniques are outlined in this section.

The membrane resistance, R_m, was measured by conducting membrane filtration tests employing deionized distilled water as the feed solution. The permeate fluxes in these tests remained constant with time, and were 1.557×10^{-5} $m^3/m^2/s$ and 2.557×10^{-5} $m^3/m^2/s$ for the NF-45 and NF-70 membranes, respectively, corresponding to a transmembrane pressure of 1,000 kPa. The membrane resistances, R_m, determined from Eq. 7, for NF-45 and NF-70 membranes were 6.412×10^{13} and 3.913×10^{13} m^{-1}, respectively. These estimates showed that the NF-45 membrane offered a higher membrane resistance than the NF-70 membrane.

Several investigators, including Nabetani and coworkers (1990), and Haynes et al. (1992), had observed that the osmotic pressure ($\Delta\pi$) could be expressed by the empirical relationship of Eq. 9. The osmometer tests conducted in this investigation facilitated the determination of osmotic pressures corresponding to different solution concentrations. These test results demonstrated the fact that osmotic pressures for tannic acid solutions were negligible in comparison with the applied transmembrane pressures (750 to 1500 kPa). Therefore, the total driving force for the tannic acid with nanofiltration in the proposed model was only represented by the transmembrane pressure.

The total resistance R_{Total} was estimated from the relation $R_{Total}=\Delta P/(\mu\cdot J_v)$, where ΔP represents the transmembrane pressure, and μ denotes the dynamic viscosity. The concentration-polarization-layer resistance R_{cp} was determined using the empirical relationship in Eq. 11. The constants were estimated by conducting the membrane tests using different feed solute concentrations, and varying the applied transmembrane pressures as well as cross-flow rates. From the test data, the values of v, ΔP, R_{Total}, C_b and C_f were determined. The constants a, b, c d, and e can be estimated by multiple regression, where it is assumed that gel-layer resistance does not exist ($R_g=0$) at the commencement of membrane operations ($t=0$). From the membrane performance test results, the constants a, b, c, d, and e were estimated as 3.80×10^{-16}, -3.02, 3.65, -3.18, and 3.18, respectively, for the NF-45 membrane, the corresponding constants for the NF-70 membrane were 3.75×10^{-53}, -6.89, 8.30, 5.0, and -5.0, respectively.

The gel-layer resistance, R_g, was evaluated from Eqs. 7 and 11 using the relation

$$R_g = R_{Total} - R_m - R_{cp} = R_{total} - R_m - a v^b \Delta P^c C_b^d C_f^e \quad (28)$$

In order to estimate the temporal variation in gel-layer resistance (dR_g/dt), a nonlinear curve-fitting method was used to fit the data. A fourth-order polynomial approximation was employed for representing R_g, and dR_g/dt was estimated from the differentiated form of Eq. 29, as shown below

$$R_g = a_0 + a_1 t + a_2 t^2 + a_3 t^3 + a_4 t^4 \quad (29)$$

and

$$dR_g/dt = a_1 + a_2 t + a_3 t^2 + a_4 t^3. \quad (30)$$

The concentration of gel layer, C_g, and the ratio of specific resistance (ϵ) and gel-layer density (ρ_g) were evaluated from a modification of Eq. 15, as shown under

$$\frac{dR_g}{dt} = A_1 C_b J_v + A_2 C_b \ln C_b + A_3 C_b, \quad (31)$$

where

$$A_1 = \frac{\epsilon}{\rho_g}, \qquad A_2 = \frac{\epsilon}{\rho_g} k, \qquad \text{and} \qquad A_3 = -\frac{\epsilon}{\rho_g} k \ln C_g.$$

The parameters, namely k, ϵ/ρ_g, and C_g, were determined from the preceding relationship using experimental data. The values of dR_g/dt, J_v, and C_b were calculated, while the parameters A_1, A_2, and A_3 were estimated by multiple regression using experimental data from several runs. The estimated values of ϵ/ρ_g and C_g were 1.54×10^{16} m/kg and 0.10 kg/m^3, respectively. The mass-transfer coefficients were also determined either from Eq. 23 or from Eqs. 17 through 19. It must be noted that the membrane performance tests were conducted under laminar flow conditions, and so estimates of mass-transfer coefficients varied between 1.28×10^{-6} and 1.68×10^{-5} m/s, depending on fluid dynamic regimes and operation conditions. The resistances R_{cp} and R_g were estimated using regression techniques on experimental data. The regression parameters a, b, c, d, and e based on Eqs. 11 and 12 were estimated using experimental data (corresponding to $t=0^+$ in the neighborhood of 1 to 3 min), for determining the resistance, R_{cp}. Similarly, the regression parameters a_0, a_1, a_2, a_3, and a_4 were estimated from Eqs. 29 and 30 for determining the resistance, R_g. Aqueous diffusion coefficient of tannic acid in dilute solution was estimated by the Stokes-Einstein equation shown in Eq. 16 and was equal to 2.64×10^{-10} m^2/s. The input parameters for the proposed membrane transport model are listed in Table 2.

It must be noted that the parameters associated with concentration polarization and gel-layer formation cannot be estimated with reliability for complex solute–solvent and membrane systems from equations without using experimental

Table 2. Entry Values for Model Parameters

Parameter	Symbol (unit)	Value
Feed solution conc.	C_f (kg/m^3)	0.0025
Gel-layer conc.	C_g (kg/m^3)	0.1
Applied pres.	ΔP (Pa)	$1.00\times10^{+6}$
Diffusion coeff.	D (m^2/s)	2.64×10^{-10}
Mass-transfer coeff.	k (m/s)	1.28×10^{-6}
Cross-flow rate	υ (m/s)	4.81×10^{-3}
Solution dynamic vis.	μ (Pa·s)	1.002×10^{-3}
Resist. of memb.	R_m (1/m)	6.41×10^{13}
Resist. per unit of L_g/gel-layer dens.	ϵ/ρ_g (m/kg)	1.54×10^{16}
Memb. surface area	A_m (m^2)	0.0155
Memb. cell cross-section area	A_c (m^2)	0.000125
Coef. for resistance of conc. polarization layer	a	3.8×10^{-16}
	b	−3.02
	c	3.65
	d	−3.18
	e	3.18

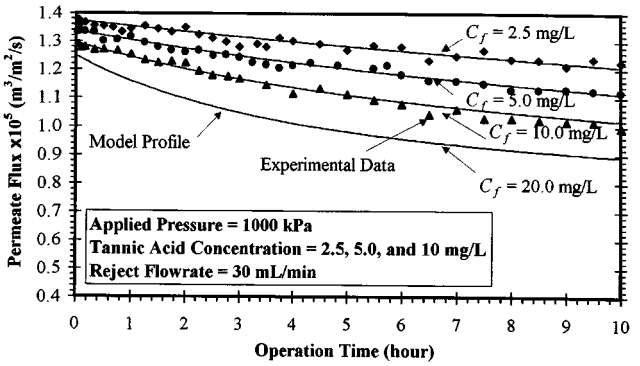

Figure 4. Model predictions vs. experimental data: NF-45 membrane for nanofiltration of tannic acid: effect of tannic acid concentration in feed solution.

data. Additionally, due to the complex structure of tannic acid, and the proprietary nature of commercial membrane materials, regression techniques represented the only well-established, reliable, accurate, and flexible *modus operandi* for estimating the resistances R_{cp} and R_g from experimental data. Furthermore, a large number of data points was used for maintaining a high degree of statistical freedom and reliability in these estimations.

Model predictions/simulations

Complete removal of tannic acid was achieved in all the membrane filtration experiments. This was expected because the cutoff sizes of NF-45 and NF-70 nanofiltration membranes were about 300 Daltons, significantly lower than the molecular weight of tannic acid of about 1,700 Daltons. This observation provided sufficient justification for employing a membrane transport model without internal pore fouling for simulating the permeate flux.

Model predictions were obtained for the permeate flux and compared with the experimental data. Variations in important operating conditions, including the feed concentration, transmembrane pressure, and reject flow rate, were attempted to investigate their influences on permeate flux patterns. The operating conditions for each set of membrane filtration experiments (NF-45 and NF-70) are summarized in Table 3, and the corresponding experimental and predicted profiles are presented in Figures 4 through 9. In all cases, comparisons of experimental data and model predictions for permeate fluxes demonstrate a good agreement, establishing that the model has excellent predictive capability under various operating conditions.

Table 3. Membrane Operating Conditions for Transport Model Verification

	Transmembrane Pres. (ΔP, kPa)	Feed Solute Conc. (mg/L)	Reject Flow rate (mL/min)	Figure No.
NF-45				
Exp. 1	1,000	2.5, 5, 10	30	4
Exp. 2	750, 1,000, 1,500	10	30	5
Exp. 3	1,500	10	30, 40, 50	6
NF-70				
Exp. 4	1,000	2.5, 5, 10	30	7
Exp. 5	750, 1,000, 1,500	10	30	8
Exp. 6	1,000	10	30, 40, 50	9

Membrane filtration experiments

The experimental data of permeate flux for NF-45 membranes are presented in Figures 4 through 6. The membrane experiments were conducted by varying several operating conditions, including the tannic acid feed concentration, transmembrane pressure, and reject flow rate. The results depicted in Figure 4 correspond to the NF-45 membrane experiments for tannic acid feed concentrations of 2.5, 5, and 10 mg/L, respectively. In these experimental runs, the other operating conditions were identical; the transmembrane pressure was 1,000 kPa, the reject flow rate was maintained at 30 mL/min, and the duration of each run was 10 h. The results indicate that the permeate flux reductions after 10 h of operation were 10.9%, 16.1%, and 22.8% for progressively increasing tannic acid concentrations of 2.5, 5, and 10 mg/L, respectively. The results observed in these experimental runs

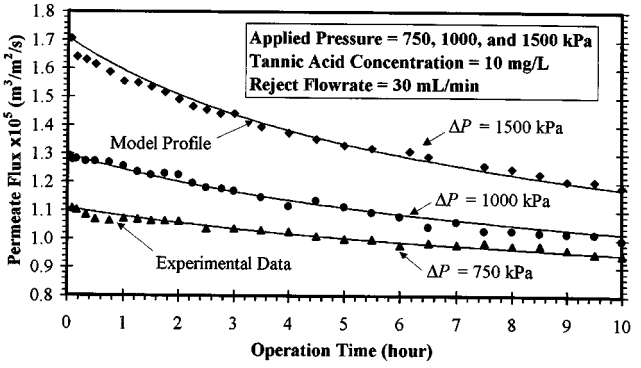

Figure 5. Model prediction vs. experimental data: NF-45 membrane for nanofiltration of tannic acid: effect of transmembrane pressure.

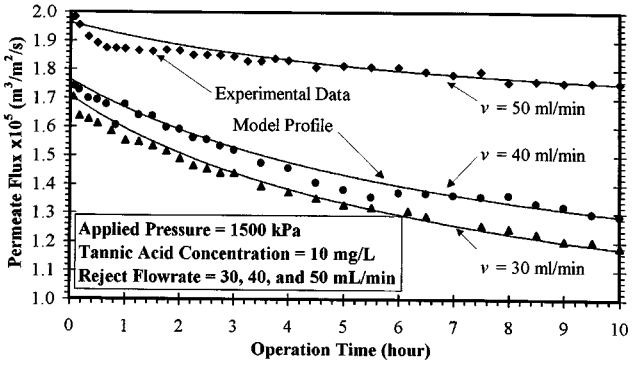

Figure 6. Model predictions vs. experimental data: NF-45 membrane for nanofiltration of tannic acid: effect of reject flow rate.

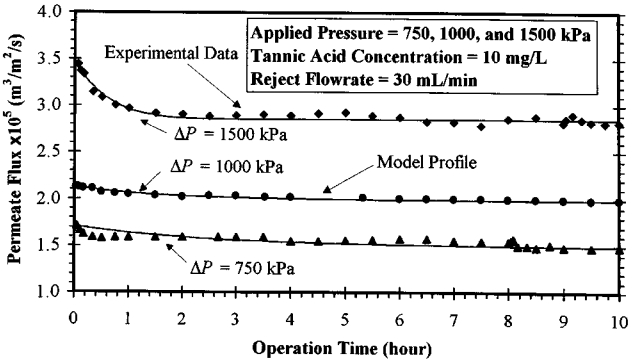

Figure 8. Model predictions vs. experimental data: NF-70 membrane for nanofiltration of tannic acid: effect of transmembrane pressure.

for the NF-45 membrane can be qualitatively explained by the differences in the gel-layer resistances corresponding to different initial solute concentrations. The permeate flux decline manifests an exponential relationship that is approximately linear during the operation period of 10 h. However, the rate of flux decline with time exhibits a substantial increase at higher solute concentrations. This can be attributed to the fact that the thickness of gel-layer formation by surface adsorption and/or internal pore adsorption is a monotonically increasing function of solute concentration. On a related note, the initial permeate flux (permeate flux at $t = 0$) is reduced when the membrane is exposed to a higher solute concentration. This observation substantiates the argument that adsorption of solute molecules on the membrane occurs instantaneously when the membrane is exposed to the feed solution, and the gel layer is formed, and the initial gel-layer thickness is dependent on the solute concentration. Subsequently, as the gel-layer thickness increases, greater reductions in permeate fluxes are experienced at higher solute concentrations.

The results depicted in Figure 5 correspond to the NF-45 membrane experiments for various transmembrane pressures. It can be seen that with a tannic acid feed concentration of 10 mg/L, fractional permeate flux reductions of 14.6%, 22.8%, and 30.6% were experienced, corresponding to transmembrane pressures of 750, 1,000 and 1,500 kPa, respectively. Although the intrinsic permeate fluxes were greater at higher transmembrane pressures (due to the greater driving force), the fractional permeate flux reductions were quantitatively increased at higher transmembrane pressures. A qualitative explanation for this observed behavioral pattern is that at higher transmembrane pressures, the gel layer becomes more compacted as filtration progresses, building up higher solvent mass-transfer resistance, and consequently, leading to a faster deterioration in permeate flux.

The results depicted in Figure 6 correspond to the NF-45 membrane experiments under the following conditions: tannic acid feed concentration of 10 mg/L, transmembrane pressure of 1500 kPa, and different reject flow rates. These experiments were intended to evaluate the effect of reject flow rate on the permeate flux. The results indicated that the permeate flux reductions after 10 h of operation were 30.6%, 25.9%, and 11.4%, corresponding to reject flow rates of 30, 40, and 50 mL/min, respectively. It should also be noted that the initial permeate fluxes were greater at higher reject flow rates. Increasing the reject flow rate (or the cross-flow rate) results in slower accumulation of gel material on the membrane surface, and consequently leads to a thinner gel layer

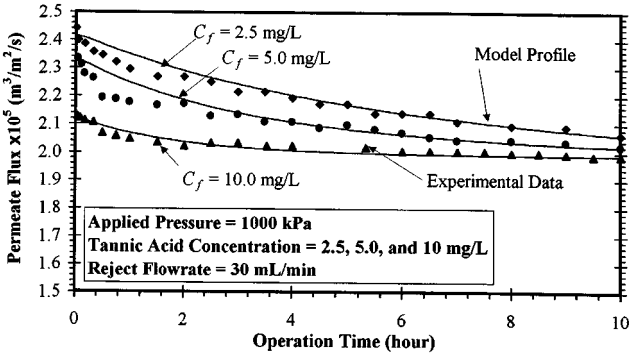

Figure 7. Model predictions vs. experimental data: NF-70 membrane for nanofiltration of tannic acid: effect of tannic acid concentration in feed solution.

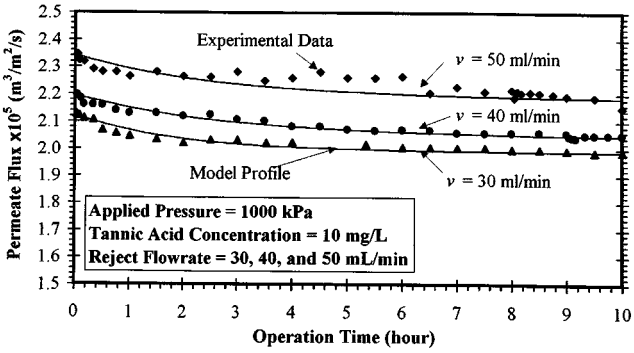

Figure 9. Model predictions vs. experimental data: NF-70 membrane for nanofiltration of tannic acid: effect of reject flow rate.

Table 4. Important Hydrodynamic Properties of the Fluid Under Experimental Conditions

Parameter	NF-45 and NF-70 Membranes		
Reject flow rate (mL/min)	30	40	50
Permeate flux ($m^3/m^2/s$)	1.71×10^{-5}	1.76×10^{-5}	1.96×10^{-5}
Reynolds No.	4.0	4.9	5.9
Peclet No.	15,000	18,400	22,300
$\delta_{BL/h}$	0.215	0.201	0.188
f(%)	1.46	1.19	0.99
C_{BL}/C_0	78	61	44

after several hours of operation. Thus, the lower fractional reduction in permeate flux observed at higher reject flow rate can be attributed to the lower gel-layer resistance associated with slower gel formation. However, the increased initial permeate flux corresponding to higher reject flow rate cannot be qualitatively explained by the ''slower gel formation'' theory, but can only be accounted for by the ''boundary layer'' theory. A graphical illustration of the boundary-layer phenomenon is provided in Figure 2b. It must be noted that at a higher reject flow rate, the tangential fluid velocity at the membrane surface is greater, resulting in a thinner hydrodynamic boundary layer. This leads to a higher back-diffusion mass-transfer rate of the gel material, and possibly results in the formation of a thinner gel layer during the first few seconds of membrane exposure to the solute molecules (foulant molecules) in the experimental run.

Estimation of boundary-layer thickness and concentration factors

It can be observed from Table 4 that a relatively thick hydrodynamic boundary layer forms ($\delta_{BL}/h^* \approx 0.2$) under the low-velocity flow regime ($Re < 6$). The dimensionless thickness decreases with larger Reynolds numbers, corresponding to higher reject flow rates. It is also evident that a relatively small fraction of feed ($f < 1.5\%$) flows through the boundary layer; however, the solute concentration in the boundary layer is substantially greater than that in the feed. Such a high boundary-layer solute concentration apparently poses significant impact on subsequent polarization and gel-layer formation, because it causes initial buildup of a dense layer of molecules near the membrane surface. As the flow rate increases, however, the boundary-layer concentration decreases, facilitating greater mass transfer and permeate flux enhancement. This observation offers an explanation as to why the initial permeate flux increases at higher reject flow rates in the experimental runs.

Prediction of permeate flux under different operating conditions

The experimental data for the NF-70 membrane permeate fluxes under different operating conditions are presented in Figures 7 through 9. The results depicted in Figure 7 correspond to different tannic acid feed concentrations. Other operating conditions were held identical, as depicted in Table 3. The permeate flux reductions after 10 h of operation were 15.5%, 13.4%, and 6.5%, corresponding to tannic acid feed concentrations of 2.5, 5 and 10 mg/L, respectively. This behavioral pattern was qualitatively similar to that observed for the NF-45 membrane (Figure 4), and can therefore be explained by the same theory.

The results depicted in Figure 8 correspond to the NF-70 membrane experiments for a tannic acid feed concentration of 10 mg/L at different transmembrane pressures. Figure 8 shows that the permeate flux reductions were estimated at 6.3%, 6.6%, and 18.9%, corresponding to transmembrane pressures of 750, 1,000 and 1,500 kPa, respectively. The greater reduction in permeate flux observed at higher transmembrane pressures could be attributed to the greater compaction of the gel layer, which is qualitatively similar to the explanation offered for the NF-45 membrane.

The results presented in Figure 9 correspond to the NF-70 membrane experiments for various reject flow rates. The data indicate that the permeate flux reductions were 6.5%, 6.6%, and 8.3%, corresponding to reject flow rates of 30, 40 and 50 mL/min, respectively. Similar to NF-45 membrane experiment results, increasing the reject flow rate resulted in higher permeate flux, and this could be explained by possible reduction in gel-layer thickness at higher cross-flow rates across the membrane surface. However, the permeate flux reduction remained almost unchanged under various reject flow rates, and the effects were less significant than those observed for NF-45 membranes. This could be attributed to the lower sorption affinity of tannic acid for the NF-70 membrane than for the NF-45 membrane, resulting in a lower gel-layer formation rate, and consequently lower mass-transfer resistance in the former. This explanation is also substantiated (both qualitatively and quantitatively) by comparison of permeate flux results for the NF-45 and NF-70 membranes.

Comparisons of permeate flux profiles for NF-45 and NF-70 membranes under similar operating conditions (comparisons of Figures 4 and 7, Figures 5 and 8, and Figures 6 and 9) clearly indicate that the initial permeate fluxes were higher for the latter. The rates of flux decline due to increased solute concentrations or transmembrane pressure were also more pronounced in the case of NF-45 membranes. The quantitative values of fractional permeate flux reduction for both membranes under identical conditions are summarized in Table 5. The NF-70 maintains an inherently higher water

Table 5. Relative Flux Decline between NF-45 and NF-70 Membranes

Variable		Rel. Flux Decline (%) after 10-h Oper. NF-45	NF-70
$\Delta P = 1{,}000$ kPa	C_f (mg/L)		
$Q_{rej} = 30$ mL/min	2.5	10.9	15.5
	5.0	16.1	13.4
	10.0	22.8	6.5
$C_f = 10.0$ mg/L	ΔP (kPa)		
$Q_{rej} = 30$ mL/min	750	14.6	6.3
	1,000	22.8	6.6
	1,500	30.6	18.9
$C_f = 10.0$ mg/L	Q_{rej} (mL/min)	$\Delta P = 1{,}500$ kPa	$\Delta P = 1{,}000$ kPa
	30	30.6	6.5
	40	25.9	6.6
	50	11.4	8.3

Key: C_f = feed tannic acid concentration; ΔP = applied transmembrane pressure; Q_{rej} = reject flow rate

flux of more than 60% compared to that of the NF-45 membrane. Although both membrane surfaces are composed of polyamide materials, the exact information regarding their compositions is not available. It is hence difficult to attribute the initial flux difference to any particular characteristic of the membrane. However, the flux variation is clearly influenced by the membrane surface chemistry involving its material hydrophobicity. In general, hydrophilic membrane surfaces facilitate water transport by forming hydrogen bonds with the water molecules, and thus generate a higher permeate flux than hydrophobic membrane surfaces. In this study, we measured the contact angle for both membranes to estimate their relative hydrophilicity. The results presented in Table 1 indicate that NF-45 is consistently more hydrophobic than NF-70, as reflected by the larger contact angles of the former. Therefore, our experimental results are consistent with this hypothesis, manifesting a higher permeate flux for NF-70 than for NF-45 membranes.

Membrane fouling is generally explained by the phenomena of boundary-layer development and gel-layer formation, as previously discussed. However, the "fouling potential" of a membrane is greatly influenced by its surface characteristics. Three major factors are generally believed to contribute to the flux-decline phenomenon: (1) sorption of organic molecules on membrane surface, (2) chemical interactions between membrane surface and the organic molecules, and (3) electrostatic interactions between membrane surface and the organic molecules. Physical adsorption of organic molecules on the hydrophobic sites of the membrane surface is an important factor with reference to organic rejection, but its effects on permeate flux is highly dependent on whether polymer–organic molecule interactions occur. The fact that NF-45 membrane exhibits greater affinity to tannic acid adsorption (Tu et al., 1997) apparently has immense impact on its greater flux decline as compared to the NF-70 membrane, due to chemical interactions between the adsorbed tannic acid molecules and the hydrophilic polymer sites. This is because water should be preferentially sorbed by the membrane polymer to allow high water fluxes. However, the organic molecules capable of forming stronger hydrogen bonds will displace water molecules from the hydrophilic sites of the membrane, and thus impede water transport though the thin-film polymeric layer. Examples of such interactions for the NF-45 and NF-70 membranes are presented in Figures 10 and 11, respectively. These figures illustrate the potential for hydrogen bond formation between the carbonyl group of the polymeric surfaces of the two membranes with the phenolic hydroxyl group in the tannic acid molecules. These strong hydrogen bonds are practically irreversible, and possibly contribute to the rapid accumulation of gel material in subsequent stages.

The differences in the affinities of NF-45 and NF-70 membranes for tannic acid adsorption due to solute–membrane interactions can be illustrated by surface charge or surface-potential (zeta potential) measurements. The surface-potential data for the two types of membranes in the pH range of 6 to 9 corresponding to deionized distilled water and 10 mg/L tannic acid, are presented in Table 1. It must be noted that the charged phenolic groups in tannic acid and the carbonyl groups in the membrane polymer dictate the overall surface charge. Under low pH conditions, the membrane surfaces

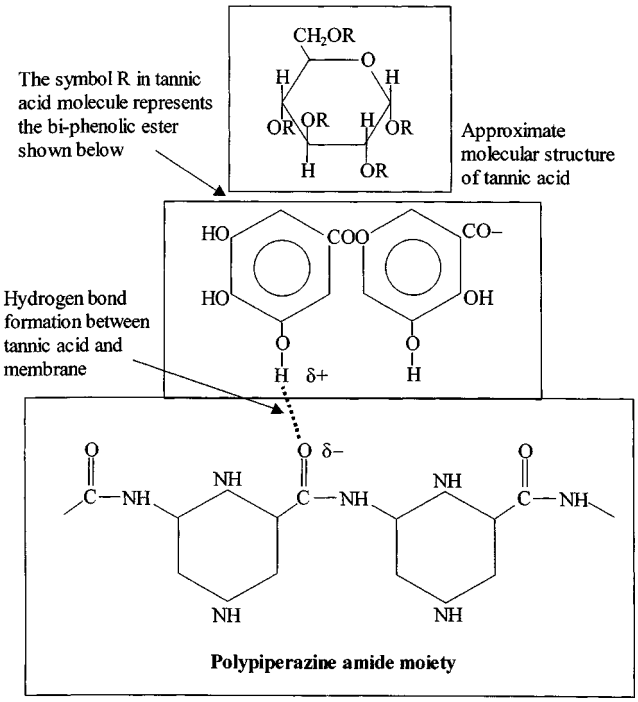

Figure 10. Interactions between NF-45 polypiperazine amide membrane and tannic acid.

have positive charges, and consequently maintain a positive surface potential. At higher pH ranges beyond their isoelectric points, both membranes maintain negative surface

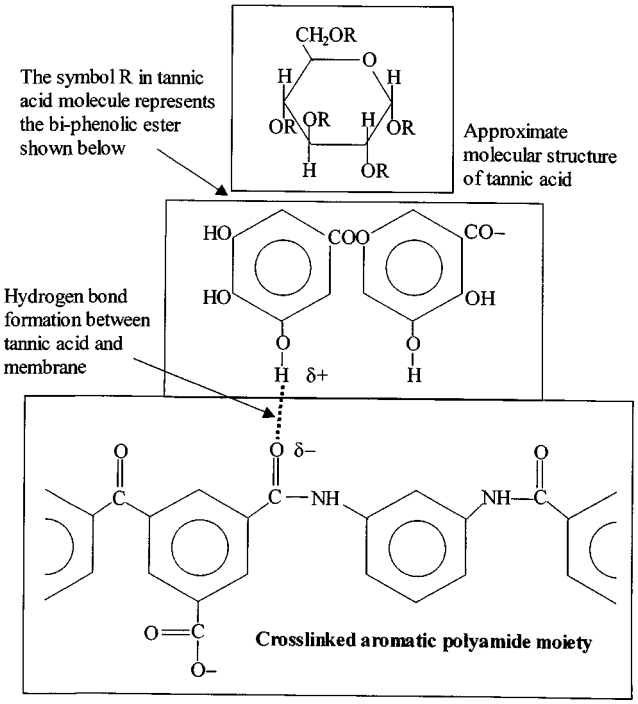

Figure 11. Interactions between NF-70 cross-linked aromatic polyamide membrane and tannic acid.

Table 6. Contributions of Various Resistances under Different Operating Conditions for NF-45 membrane

Reject Flow Rate (mL/min)	Appl. Pres. (kPa)	Feed Solute Conc. (mg/L)	Oper. Time (h)	$R_{cp}\times10^{-12}$ (m^{-1})	$R_g\times10^{-12}$ (m^{-1})	$R_{Total}\times10^{-12}$ (m^{-1})	α_m	α_{cp}	α_g
			0	9.0	0	73.1	0.88	0.12	0.00
30	1,000	2.5	5	10.1	3.9	78.1	0.82	0.13	0.05
			10	10.8	6.9	81.8	0.78	0.13	0.08
			0	10.4	0	74.5	0.86	0.14	0.00
30	1,000	5	5	12.1	7.2	83.4	0.77	0.15	0.09
			10	13.1	12.1	89.3	0.72	0.15	0.14
			0	13.2	0	77.3	0.83	0.17	0.00
30	1,000	10	5	15.6	10.9	90.6	0.71	0.17	0.12
			10	16.8	16.7	97.6	0.66	0.17	0.17
			0	23.9	0	88.0	0.73	0.27	0.00
30	1,500	10	5	35.4	14.1	113.6	0.56	0.31	0.12
			10	39.6	19.3	123.0	0.52	0.32	0.16
			0	21.1	0	85.3	0.75	0.25	0.00
40	1,500	10	5	27.2	14.9	106.2	0.60	0.26	0.14
			10	29.7	21.7	115.5	0.55	0.26	0.19
			0	11.6	0	75.7	0.85	0.15	0.00
50	1,500	10	5	12.9	5.9	82.9	0.77	0.16	0.07
			10	13.4	7.8	85.3	0.75	0.16	0.09

Key: $R_m = 64.1\times10^{12}\,m^{-1}$.

charges, mainly contributed by the charged phenolic groups generated by hydrolysis of tannic acid. However, there are differences in surface charge contributions of carboxyl groups on the NF-45 and NF-70 membranes, mainly arising from their material properties. The NF-45 membrane is composed of polypiperazine amide blocks (Figure 10), while the NF-70 membrane is composed of cross-linked aromatic polyamide blocks (Figure 11). The hydrolyzability of carboxyl groups in the two types of membrane polymers and their negative charge contributions determine the differences in their hydrophobic or hydrophilic characteristics. The surface-charge contributions of the carboxyl groups are similar for both membranes in the presence of deionized distilled water, and the surface potentials for both membranes for a pH range of 6 to 9 vary from -22 mV to -33 mV, as presented in Table 1. However, the surface potentials are distinctly different for the two membranes in the presence of 10 mg/L tannic acid, demonstrating the significance of solute–membrane interactions. The surface potentials for the NF-45 membrane vary from -14 mV to -18 mV for a pH range of 6 to 9, while those for the NF-70 membrane corresponding to the same pH range vary from -34 mV to -40 mV, as shown in Table 1. These observations can be explained by the hydrolyzability of carboxyl groups in the membrane polymers. The carboxyl groups in the polypiperazine amide blocks constituting the NF-45 membrane are not easily amenable to hydrolysis in the presence of tannic acid to make significant negative surface-charge or surface-potential contributions. On the other hand, the carboxyl groups of cross-linked aromatic polyamide blocks of the NF-70 membrane are hydrolyzed more easily under

Table 7. Contributions of Various Resistance under Different Operating Conditions for NF-70 Membrane

Reject Flow Rate (mL/min)	Appl. Pres. (kPa)	Feed Solute Conc. (mg/L)	Oper. Time (h)	$R_{cp}\times10^{-12}$ (m^{-1})	$R_g\times10^{-12}$ (m^{-1})	$R_{Total}\times10^{-12}$ (m^{-1})	α_m	α_{cp}	α_g
			0	2.2	0	41.2	0.95	0.05	0.00
30	1,000	2.5	5	2.4	4.6	46.0	0.85	0.05	0.10
			10	2.6	6.8	48.4	0.81	0.05	0.14
			0	3.7	0	42.7	0.91	0.09	0.00
30	1,000	5	5	3.9	5.0	47.9	0.81	0.08	0.10
			10	4.0	6.3	49.3	0.79	0.08	0.13
			0	7.8	0	46.8	0.83	0.17	0.00
30	1,000	10	5	8.1	2.7	49.8	0.78	0.16	0.05
			10	8.2	3.0	50.2	0.78	0.16	0.06
			0	4.5	0	43.5	0.90	0.10	0.00
30	1,500	10	5	8.4	5.0	52.4	0.74	0.16	0.10
			10	8.4	5.0	52.4	0.74	0.16	0.10
			0	6.4	0	45.4	0.86	0.14	0.00
40	1,000	10	5	6.4	2.7	48.1	0.81	0.13	0.06
			10	6.4	3.3	48.7	0.80	0.13	0.07
			0	3.5	0	42.5	0.92	0.08	0.00
50	1,000	10	5	3.6	2.6	45.2	0.86	0.08	0.06
			10	3.6	3.0	45.6	0.86	0.08	0.07

Key: $= 39.0\times10^{12}\,m^{-1}$.

the preceding conditions, and contribute to larger magnitudes of negative surface potentials. The NF-70 membrane with large magnitudes of negative surface potentials has a poorer affinity for negatively charged colloids or organic molecules such as tannic acid than the NF-45 membrane, and is therefore less amenable to organic or colloidal fouling. The surface potential data also suggest that the NF-45 membrane is less hydrophilic than the NF-70 membrane, and is therefore more susceptible to organic fouling by tannic acid. Thus, the results from surface potential studies appear to be consistent with the observation that hydrophobic membranes are generally more sensitive to adsorption of polar organic molecules than hydrophilic membranes (Crozes et al., 1993; Williams et al., 1999).

Contributions of various resistances under different operating conditions

An important objective of the membrane transport model was to estimate the relative contributions of various mass-transfer resistances attributed to the membrane layer (R_m), concentration polarization layer (R_{cp}), and gel layer (R_g), to the total resistance (R_{Total} under different conditions, including the feed solute (tannic acid) concentration, reject flow rate, transmembrane pressure, and operating time. The fractional contribution of R_m, R_{cp}, and R_g to the total resistance R_{Total} are denoted by α_m, α_{cp}, and α_g, respectively. The various resistances and their relative fractional contributions under different operating conditions are shown in Tables 6 and 7 for NF-45 and NF-70 membranes, respectively.

The resistance R_m is an inherent characteristics invariant for each membrane, and is a major contributor to R_{Total}. However, resistances R_{cp} and R_g manifest variations with operation time, solute concentrations, reject flow rate, and transmembrane pressure. The estimates presented in Table 6 for the NF-45 membrane shows that R_g progressively increases with time, and the increment is proportional to feed solute concentration. Resistance R_{cp} manifests similar increases for the NF-45 membrane at a transmembrane pressure of 1,000 kPa. However, when pressure is increased from 1,000 kPa to 1,500 kPa, under the same flow rate and solute concentration, the R_{cp} increases substantially, while R_g undergoes smaller increments; and R_{cp} is significantly greater than R_g at this point. As filtration progresses, the R_g impact becomes more significant due to gel formation, especially noticeable at high reject flow rates. However, as the reject flow rate is progressively increased from 30 mL/min to 50 mL/min, R_{cp} and R_g values undergo a dramatic reduction of 30–40%.

The estimates of resistances and their relative fractional contributions for the NF-70 membrane in Table 7 present a qualitatively different picture as compared to those for the NF-45 membrane. The R_m for the NF-70 membrane is 39.0×10^{12} m^{-1}, significantly lower than 64.1×10^{12} m^{-1} for the NF-45 membrane, consistent with its material characteristics. It must be noted that the polypiperazine membrane (NF-45) is less porous than the cross-linked aromatic polyamide membrane (NF-70), and therefore offers more resistance to fluid transport. Additionally, the polypiperazine membrane is more hydrophobic than the cross-linked aromatic polyamide membrane, and is therefore susceptible to lower solvent transport and greater organic fouling by tannic acid. It is evident from Table 7 that R_g is generally low for NF-70 membranes, and gradually increases with operation time due to gel-layer formation, but progressively decreases with feed solute concentration because of its lower tendency to adsorb foulant molecules. The R_{cp} contributions are comparable to the R_g contributions, and increase progressively with feed solute concentration. It can also be seen that increasing the transmembrane pressure from 1,000 kPa to 1,500 kPa showed a marginal increase in R_{cp} and R_g. Increase in the reject flow rates progressively from 30 mL/min to 40 mL/min and subsequently to 50 mL/min resulted in a gradual decrease in the R_{cp} and R_g values. It must be noted that the R_{cp} and R_g account for less than 15–25%, while R_m represents 75–85% of the total resistance. The progressive reduction in R_g with solute concentration can be explained by the fact that the hydrophilic NF-70 membrane tends to accumulate a thinner gel layer than the more hydrophobic NF-45 membrane under identical conditions owing to lower sorption of tannic acid. Additionally, the back diffusion is greater in the case of NF-70 due to its tendency to repel the tannic acid molecules. This argument also qualitatively explains higher levels of R_{cp} experienced in NF-45 membranes. At higher reject flow rates of 40 mL/min and 50 mL/min, R_{cp} values decrease for both membranes, indicating the significant effect of fluid turbulence on reducing resistances, although it is more pronounced in NF-45 membranes. Furthermore, NF-70 membranes do not manifest much variations of R_{cp} and R_g with operating time as compared to NF-45 membranes. This can possibly be attributed to the hydrophilic nature of the former, and consequently its lower tendency to form the concentration polarization and gel layers.

Model sensitivity analysis

Model sensitivity analyses were conducted to obtain a quantitative evaluation of the influence of the input parameters on the membrane transport model simulations. Such a technique can also demonstrate the significance of obtaining accurate parameter values to offer reliable predictions of the process dynamics. Figures 12 through 15 show the permeate flux predictions for tannic acid using NF-45 membranes with variations in several input parameters, including the mass-transfer coefficient (k), solution viscosity (μ), resistance per

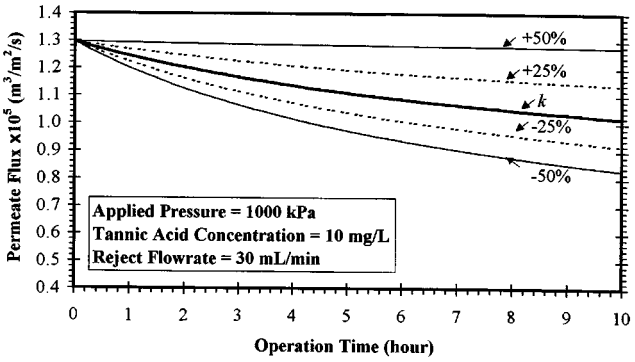

Figure 12. Model simulation for tannic acid using NF-45 membrane: effect of mass-transfer coefficient, *k*.

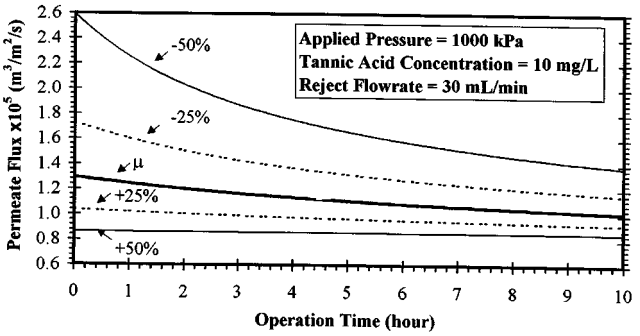

Figure 13. Model simulation for tannic acid using NF-45 membrane: effect of the solution dynamic viscosity, μ.

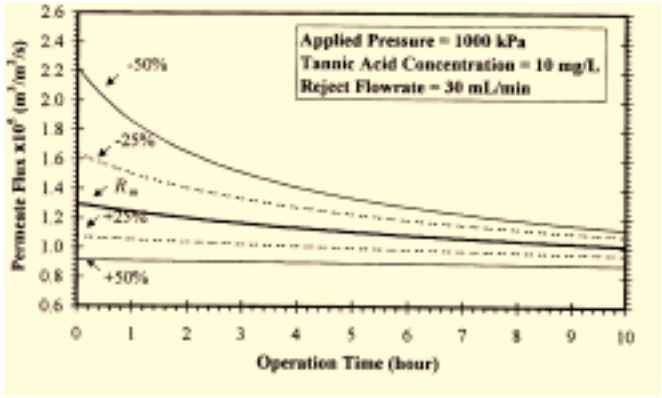

Figure 15. Model simulation for tannic acid using NF-45 membrane: effect of membrane resistance, R_m.

unit of gel-layer thickness (ϵ), and membrane resistance (R_m). These parameters represent the influences of variations in the hydrodynamic properties (k and μ), membrane properties (R_m), as well as the gel-layer properties (ϵ).

It can be observed from Figure 12 that variations in the mass-transfer coefficient due to changes in the fluid dynamics have a marked effect on permeate flux profiles. The mass-transfer coefficient is strongly influenced by several factors, including cross-flow rate, solute diffusivity, and operating temperature. Increase of the mass-transfer coefficient directly leads to an increase of the Sherwood and Reynolds numbers (Eq. 17). Consequently, the growth of gel-layer formation is minimized due to the mounting effects of forced convection, resulting in permeate flux increase. It is indeed clear that, when the cross-flow rate was increased by 50%, the mass-transfer coefficient would increase by 14%. Similarly, if the diffusion coefficient were increased by 50%, the mass-transfer coefficient would increase by 31%. The simulation results depicted in Figure 13 illustrates the effects of solution viscosity (μ). In contrast to the mass-transfer coefficient, an increase in the dynamic viscosity leads to smaller Reynolds numbers. Hence, the permeate flux declines due to increased gel-layer formation. It should be noted that the greatest impact of viscosity is observed during the initial stages of membrane operation, which implies that intrinsic fluid properties can be a major influencing factor at this point. However, as the membrane operation progresses, the impact of viscosity gradually decreases because the influences of other variables (such as mass-transfer resistance attributed to gel-layer formation) become increasingly significant, until a pseudo steady state is eventually reached.

The simulated profiles presented in Figures 14 and 15 correspond to the effects of solution resistance per unit of gel-layer thickness (ϵ) and membrane resistance (R_m), respectively. It is evident from the results depicted in Figure 14 that the permeate flux predictions were only marginally affected by variations in ϵ. An increase of 50% leads to approximately 6% of permeate flux reduction after 10 h of operation. Similarly, the effects of variation in R_m were only marginal under steady-state conditions. As described earlier, the intrinsic resistance of the membrane apparently determines the initial rate of permeate flux; however, its role gradually diminishes as the resistance due to gel-layer formation becomes more significant.

The results of the sensitivity analyses clearly demonstrated that the membrane performance was greatly influenced by the fluid-dynamic regime reflected in the mass-transfer coefficient and the fluid viscosity. Relatively lesser effects were experienced from variations of gel-layer and membrane resistances. These results also demonstrate the importance of precise determinations of the input parameters to maximize the predictive capability of the model.

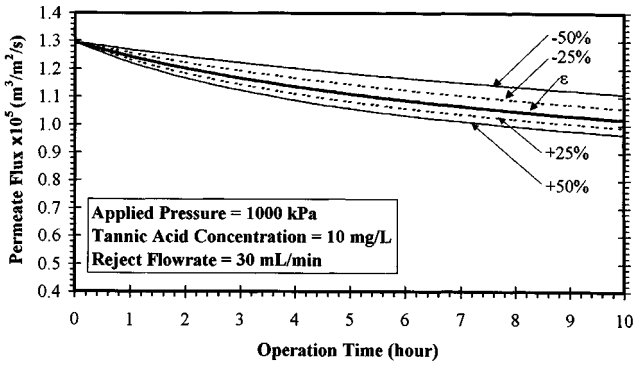

Figure 14. Model simulation for tannic acid using NF-45 membrane: effect of resistance per unit gel-layer thickness, ϵ.

Summary and Conclusions

A membrane transport model was developed to predict the permeate flux decline in nanofiltration processes under unsteady-state conditions. Nanofiltration experiments using tannic acid as a model compound for simulating natural organic matter in natural waters established the good predictive capability of the model with reference to permeate flux decline attributed to concentration polarization and gel-layer formation. The model also provided a qualitative and quantitative appreciation of the process dynamics under a variety of operating conditions.

The differences in permeate flux reduction between NF-45 and NF-70 membranes were explained on the basis of membrane surface characteristics, particularly the relative hy-

drophilicity of the thin-film polyamide surface. Apparently, the sorption of tannic acid and chemical interactions between the polar groups of membrane polymer and tannic acid molecules substantially contributed to permeate flux reduction. Membrane filtration studies demonstrated that NF-45 membranes exhibited greater affinity to tannic acid adsorption than NF-70 membranes, and thus experienced greater flux reductions. The surface potential measurements showed that NF-45 membranes were less hydrophilic and had greater affinity for tannic acid than NF-70 membranes, and were therefore more susceptible to organic fouling. The study further demonstrated that interactions between the organic solute and membrane polymers could play an important role in gel-layer formation and membrane fouling.

Tannic acid was completely removed by both NF-45 and NF-70 membranes. This was consistent with the fact that the molecular cutoff sizes of the membranes were about 300 Da, significantly lower than the molecular weight of tannic acid of about 1,700 Da.

Model sensitivity analyses demonstrated that precise determination of input parameters was of critical importance for model simulations. Higher initial permeate fluxes were observed with increases in applied pressures, decreases in feed concentrations, and/or increases in reject flow rates. The higher permeate fluxes were attributed to increases in the driving forces and decreases in the resistances of the concentration polarization layer. Also, when the applied pressure was increased, greater permeate flux reductions were observed, a factor that could be attributed to the increase in gel-layer compaction and gel-layer resistance. Furthermore, a theoretical analysis was attempted to quantify the impacts of the hydrodynamic boundary layer on the formation of concentration polarization and gel layers. The results suggested significant effects of such a boundary layer, particularly under the low-velocity flow regime experienced in this study.

Acknowledgments

The authors extend their appreciation to the following individuals for supplying membranes for this research: Mr. Chris Rollins, Vice President, Sea Recovery, Inc., Gardena, CA; and Ms. Sharon Whipple and Mr. Bill Holly, Liquid Separation Systems Division, FilmTec, Inc., Minneapolis, MN.

Notation

B_n = nth virial coefficient, $m^{3(n-1)}$ kg $^{-n+1}$
C = solute concentration, kg/m^3
C_0 = concentration at the center of the plate, kg/m^3
C_b = concentration in the bulk solution, kg/m^3
C_{BL} = concentration within the boundary layer, kg/m^3
C_f = concentration in the feed solution, kg/m^3
C_g = concentration in the gel layer, kg/m^3
C_m = concentration at the membrane surface on the bulk solution side, kg/m^3
C'_m = concentration at the membrane surface on the membrane side, kg/m^3
C_p = concentration in the permeate solution, kg/m^3
d_h = hydraulic diameter, m
D = molecular diffusion coefficient, m^2/s
f = volumetric flow fraction
h = channel height between the plate, m
J_v = permeate flux, m^3/m$^2\cdot$s
k = Boltzmann constant = $R/N = 1.38062\times10^{-23}$, J/K
k = mass-transfer coefficient, m/s
L = length of a membrane module, m
L^* = length of the entry region in the module ($L^* = 0.029 d_h Re$), m
L_g = thickness of the gel layer, m
MW = weight-average molecular weight, kg/mol
N = Avogadro's number = 6.022169×10^{23} mol^{-1}
r = molecular radius, m
R = gas-law constant = 8.3143 J$\cdot$mol$^{-1}\cdot$K^{-1}
Re = Reynolds number, $\mathrm{Re} = \rho v d_h/\mu$
R_{Total} = total resistance of the membrane, m^{-1}
R_{cp} = resistance of the concentration polarization layer, m^{-1}
R_{in} = resistance due to the internal pore fouling, m^{-1}
R_g = resistance of the gel layer, m^{-1}
R_m = resistance of the membrane, m^{-1}
Sc = Schmidt number ($Sc = \mu/\rho D$)
Sh = Sherwood number
T = absolute temperature, K
u_0 = axial flow velocity at the center of the plate, m/s
v = cross-flow velocity, m/s
V_w = permeate velocity, m/s

Greek letters

α_m = fractional contribution of membrane resistance to the total resistance
α_{cp} = fractional contribution of concentration polarization resistance to the total resistance
α_g = fractional contribution of gel-layer resistance to the total resistance
ϵ = resistance per unit of the gel layer thickness, m^{-2}
δ = thickness of the concentration polarization layer, m
δ_{BL} = boundary layer thickness, m
μ = dynamic viscosity, Pa$\cdot$s = kg$\cdot$m$^{-1}\cdot$s^{-1}
η = kinematic viscosity, m^2/s
ρ = density of the solution, kg/m^3
ρ_A = density of the molecule, kg/m^3
ρ_g = density of the gel layer, kg/m^3
ΔP = applied pressure, Pa = kg$\cdot$m$^{-1}\cdot$s^{-2}
$\Delta\pi$ = osmotic pressure between the bulk solution and the permeate, Pa

Literature Cited

Aim, B. R., M. G. Liu, and S. Vigneswaran, "Recent Development of Membrane Processes for Water and Waste Water Treatment," *Water Sci. Technol.*, **27**(10), 141 (1993).

Akay, G., and R. J. Wakeman, "Ultrafiltration and Microfiltration of Surfactant Dispersions—An Evaluation of Published Research," *Trans. Inst. Chem. Eng.*, **71**(A), 411 (1993).

Bhattacharyya, D., S. L. Back, and R. I. Kermode, "Prediction of Concentration Polarization and Flux Behavior in Reverse Osmosis by Numerical Analysis," *J. Memb. Sci.*, **48**, 231 (1990).

Bird, R. B., W. E. Stewart, and E. N. Lightfoot, *Transport Phenomena*, Wiley, New York (1960).

Braghetta, A., F. A. DiGiano, and W. P. Ball, "Nanofiltration of Natural Organic Matter: pH and Ionic Strength Effects," *J. Environ. Eng.*, **123**, 628 (1997).

Chapra, S. C., and R. P. Canale, *Numerical Methods for Engineers*, 2nd ed., McGraw-Hill, New York (1988).

Chellam, S., and M. R. Wiesner, "Particle Transport in Clean Membrane Filters in Laminar Flow," *Environ. Sci. Technol.*, **26**, 1611 (1992).

Chellam, S., and M. R. Wiesner, "Particle Back-Transport and Permeate Flux Behavior in Crossflow Membrane Filters," *Environ. Sci. Technol.*, **31**, 819 (1997).

Cornel, P., R. S. Summers, and P. V. Roberts, "Diffusion of Humic Acid in Dilute Aqueous Solution," *J. Colloid Interface Sci.*, **110**, 149 (1986).

Crozes, G., C. Anselme, and J. Mallevialle, ''Effect of Adsorption of Organic Matter on Fouling of Ultrafiltration Membranes,'' *J. Memb. Sci.*, **84**, 61 (1993).
Dentel, S. K., J. Y. Bottero, K. Khatib, H. Demougeot, J. P. Duguet, and C. Anselme, ''Sorption of Tannic Acid, Phenol, and 2,4,5-Trichlorophenol on Organoclays,'' *Water Res.*, **29**, 1273 (1995).
Doshi, M. R., ''Boundary Layer Removal in Ultrafiltration,'' *Ultrafiltration Membranes and Applications*, A. R. Cooper, ed., Plenum Press, New York, p. 231 (1980).
Fu, P., H. Ruiz, K. Thompson, and C. Spangenberg, ''Selecting Membranes for Removing NOM and DBP Precursors,'' *J. Amer. Water Works Assoc.*, **86**(12), 55 (1994).
Haynes, C. A., K. Tamura, H. R. Korfer, and J. M. Prausnitz, ''Thermodynamic Properties of Aqueous α-Chymotrypsin Solutions from Membrane Osmometry Measurements,'' *J. Phys. Chem.*, **96**, 905 (1992).
Ho, W. S. W., and K. K. Sircar, ed., *Membrane Handbook*, Van Nostrand-Reinhold, New York (1992).
Kim, S. H., and M. Pirbazari, ''Bioactive Adsorber Model for Industrial Wastewater Treatment,'' *J. Environ. Eng.*, **115**, 1235 (1989).
Ko, M. K., and J. J. Pellegrino, ''Determination of Osmotic Pressure and Fouling Resistances and their Effects on Performance of Ultrafiltration Membranes,'' *J. Memb. Sci.*, **74**, 141 (1992).
Koros, W. J., ''Membranes: Learning a Lesson from Nature,'' *Chem. Eng. Prog.*, **91**(10), 68 (1995).
Lindfield, G., and J. Penny, *Numerical Methods Using Matlab*, Horwood, New York (1995).
Mallevialle, J., C. Anselme, and O. Marsigny, ''Effects of Humic Substances on Membrane Processes,'' *Aquatic Humic Substances: Influence on Fate and Treatment of Pollutants* Advances in Chemistry Ser., No. 219, I. H. Suffet and P. MacCarthy, eds., Amer. Chem. Soc., p. 749 (1989).
Mallevialle, J., P. E. Odendaal, and M. R. Wiesner, *Water Treatment Membrane Processes*, McGraw-Hill, New York (1996).
Nabetani, H., M. Nakajima, A. Watanabe, S. Nakao, and S. Kimura, ''Effects of Osmotic Pressure and Adsorption on Ultrafiltration of Ovalbumin,'' *AIChE J.*, **36**, 907 (1990).
Nakao, S., J. G. Wijmans, and C. A. Smolders, ''Resistance to the Permeate Flux in Unstirred Ultrafiltration of Dissolved Macromolecular Solutions,'' *J. Memb. Sci.*, **26**, 165 (1986).
Pirbazari, M., B. N. Badriyha, and V. Ravindran, ''MF-PAC for Treating Waters Contaminated with Natural and Synthetic Organics,'' *J. Amer. Water Works Assoc.*, **84**(u2), 95 (1992).
Pirbazari, M., V. Ravindran, B. N. Badriyha, and S. H. Kim, ''Hybrid Membranes Filtration Process for Leachate Treatment,'' *Water Res.*, **30**, 2691 (1996).
Pradanos, P., J. I. Arribas, and A. Hernandez, ''Hydraulic Permeability, Mass Transfer, and Retention of PEGs in Cross-Flow Ultrafiltration Through a Symmetric Microporous Membrane,'' *Sep. Sci. Technol.*, **27**, 2121 (1992).
Pradanos, P., J. de Abajo, J. G. de la Campa, and A. Hernandez, ''A Comparative Analysis of Flux Limit Models for Ultrafiltration Membranes,'' *J. Memb. Sci.*, **108**, 129 (1995).
Ravindran, V., B. N. Badriyha, M. Pirbazari, and S. H. Kim, ''Modeling of Bioactive Carbon Adsorbers: A Hybrid Weighted Residual-Finite Difference Numerical Technique,'' *Appl. Math. Comput.*, **76**, 99 (1996).
Redondo, J. A., and F. Lanari, ''Membrane Selection and Design Consideration for Meeting European Potable Water Requirements Based on Different Feedwater Conditions,'' *Desalination*, **113**, 309 (1997).
Rivera-Utrilla, J., C. Moreno-Castilla, E. Utrera-Hidalgo, and F. Carrasco-Marin, ''Removal of Tannic Acid from Aqueous Solutions by Activated Carbons,'' *Chem. Eng. J.*, **52**, 37 (1993).
Sadr Ghayeni, S. B., P. J. Beatson, R. P. Schneider, and A. G. Fane, ''Water Reclamation from Municipal Wastewater Using Combined Microfiltration-Reverse Osmosis: Preliminary Performance Data and Microbiological Aspects of System Operation,'' *Desalination*, **116**, 65 (1998).
Schiesser, W. E., *The Numerical Method of Lines: Integration of Partial Differential Equations*, Academic Press, San Diego (1991).
Sewell, G., *The Numerical Solution of Ordinary and Partial Differential Equations*, Academic Press, San Diego (1988).
Smith, G. D., *Numerical Solution of Partial Differential Equations: Finite Difference Methods*, 3rd ed., Oxford Univ. Press, New York (1985).
Standard Methods for the Examination of Water and Wastewater, 19th ed., American Public Health Association, American Water Works Association, Water Pollution Control Federation, Washington, DC (1995).
Taylor, J. S., D. M. Thompson, and J. K. Carswell, ''Applying Membrane Processes to Groundwater Sources for Trihalomethane Precursor Control,'' *J. Amer. Water Works Assoc.*, **79**(8), 72 (1987).
Timmer, J. M. K., J. Kromkamp, and T. Robbertsen, ''Lactic Acid Separation from Fermentation Broths by Reverse Osmosis and Nanofiltration,'' *J. Membr. Sci.*, **92**, 185 (1994).
Trettin, D. R., and M. R. Doshi, ''Limiting Flux in Ultrafiltration of Macromolecular Solutions,'' *Chem. Eng. Commun.*, **4**, 507 (1980).
Tu, S. C., V. Ravindran, H. H. Tsai, B. E. Koel, and M. Pirbazari, ''Surface Characterization of Nanofiltration Membranes in Water Treatment Applications,'' *Proc. AIChE Meeting*, Los Angeles (1997).
van Boxtel, A. J. B., Z. E. H. Otten, and H. J. L. J. van der Linden, ''Evaluation of Process Models for Fouling Control of Reverse Osmosis of Cheese Whey,'' *J. Memb. Sci.*, **58**, 89 (1991).
van den Berg, G. B., I. G Racz, and C. A. Smolders, ''Mass Transfer Coefficients in Cross-Flow Ultrafiltration,'' *J. Memb. Sci.*, **47**, 25 (1989).
van den Berg, G. B., and C. A. Smolders, ''Flux Decline in Membrane Processes,'' *Filtr. Sep.*, **25** 115 (1988).
Van der Bruggen, B., J. Schaep, W. Maes, D. Wilms, and C. Vandecasteele, ''Nanofiltration as a Treatment Method for the Removal of Pesticides from Ground Waters,'' *Desalination*, **117**, 139 (1998).
Vilker, V. L., C. K. Colton, and K. A. Smith, ''The Osmotic Pressure of Concentrated Protein Solutions: Effect of Concentration and pH in Saline Solutions of Bovine Serum Albumin,'' *J. Colloid Interface Sci.*, **79**, 548 (1981).
von Meien, O. F., and R. Nobrega, ''Ultrafiltration Model for Partial Solute Rejection in the Limiting Flux Region,'' *J. Memb. Sci.*, **95**, 277 (1994).
Weber, W. J., Jr. and J. C. Crittenden, ''MADAM I—A Numeric Method for Design of Adsorption Systems,'' *J. Water. Pollut. Cont. Fed.*, **47**, 924 (1975).
Wiesner, M. R., and S. Chellam, ''Mass Transport Considerations for Pressure-Driven Membrane Processes,'' *J. Amer. Water. Works Assoc.*, **84**(1), 88 (1992).
Wijmans, J. G., and R. W. Baker, ''The Solution-Diffusion Model: A Review,'' *J. Membr. Sci.*, **107**, 1 (1995).
Wijmans, J. G., S. Nakao, and C. A. Smolders, ''Flux Limitation in Ultrafiltration: Osmotic Pressure Model and Gel Layer Model,'' *J. Memb. Sci.*, **20**, 115 (1984).
Wiley, D. E., C. J. D. Fell, and A. G. Fane, ''Optimization of Membrane Module Design for Brackish Water Desalination,'' *Desalination*, **52**, 249 (1985).
Williams, M. E., J. A. Hestekin, C. N. Smothers, and D. Bhattacharyya, ''Separation of Organic Pollutants by Reverse Osmosis and Nanofiltration Membrane: Mathematical Models and Experimental Verification,'' *Ind. Eng. Chem. Res.*, **38**, 3683 (1999).

Manuscript received June 9, 2000, and revision received Dec. 11, 2000.